Reaction-Path Dynamics Calculations of the $NH_3 + O(^3P)$ Hydrogen Abstraction Reaction

J. Espinosa-García*

Departamento de Química Física, Universidad de Extremadura, 06071 Badajoz, Spain

Received: March 8, 2000; In Final Form: May 11, 2000

Molecular orbital theory was used to study the stationary points on the reaction-path of the hydrogen abstraction reaction between ammonia and an oxygen atom. In the C_s symmetry, this reaction proceeds over two potential energy surfaces, $^3A'$ and $^3A''$, with a hydrogen-bonded complex in the exit channel. From the analysis of the reaction-path curvature, we find qualitatively that excitation of the NH_3 stretch and bend modes might enhance the forward rate constants and that the OH stretch and NH_2 bend modes of the products could appear vibrationally excited, although, as a result of the randomization of the energy favored by the deep hydrogen-bonded well, these modes will appear less vibrationally excited than those in other direct reactions. The total forward thermal rate constants were calculated from the sum of the calculated rate constants for the two surfaces using variational transition-state theory with semiclassical transmission coefficients over a wide temperature range, 500−2000 K. The calculated rate constants show reasonable agreement with experimental data, with a more pronounced curvature in the Arrhenius plot than in the experimental data.

1. Introduction

The chemistry of ammonia with an oxygen atom is very complex and involves many intermediate fast reactions, and in some cases, neither the products nor the rate constants are well-known. These reactions play an important role in the conversion of fuel-nitrogen to the atmospheric contaminant NO.[1]

Experimentally, the title reaction has been extensively studied using a wide variety of detection techniques and a broad range of temperatures (300−2060 K).[2−15] To clarify the discussion, this temperature range will be split into three regions. At low temperatures (T < 400 K), the reaction mechanism (H-abstraction producing NH_2 and OH or O-addition producing a NH_3O^* excited complex) is still an open question.[3,9,10,12] The largest number of studies has been performed at intermediate temperatures (500−1000 K).[4−8,11] The high degree of dispersion of the rate constant values diminishes with temperature. For example, at 500 K, the rate constants range from 1.17×10^{-14} cm^3 $molecule^{-1}$ s^{-1} (ref 6) to 3.83×10^{-15} cm^3 $molecule^{-1}$ s^{-1} (ref 11), that is, by a factor of 3. Finally, at high temperatures (T > 1000 K), there are also fewer experimental works,[2,13−15] and the most probable mechanism is the H-abstraction. Hanson and Salimian[16] proposed a value of $k(T) = 3.21 \times 10^{-11}$ exp(−4450/T) cm^3 $molecule^{-1}$ s^{-1}, in the temperature range 1000−2100 K, with error limits of 0.5K and 2.0K, that is, a factor of 4. It is important to note that, in the three temperature regions taken independently, the experimental rate constants present a linear Arrhenius plot.

The title reaction has been comprehensively reviewed by Cohen[17] and Baulch et al.[18] Cohen reviewed this reaction with particular attention to the possible effects of secondary reactions on the deduced rate constant. He finds that the available data are not sufficient to determine whether the initial step is H-atom abstraction or O-atom addition, and that the low-temperature values of the rate constant ($T \leq 400$ K) are not consistent with values deduced at higher temperatures if the reaction proceeds by H-abstraction. He recommends the expression $k(T) = (1.8 \times 10^{-18})T^{2.1}$ exp(−2620/T), with a high degree of curvature ($T^{2.1}$) in the Arrhenius plot. Finally, Baulch et al. recommend the expression $k(T) = 1.6 \times 10^{-11}$ exp(−3670/T) over the range 500−2500 K, with an error limit of $\Delta \log K = \pm 0.5$. Both surveys[17,18] agree that the best values are those of Perry[11] at intermediate temperatures [$k(T) = 3.3 \times 10^{-11}$ exp(−4530/T) over the range 448−841 K] and of Salimian et al.[14,16] at high temperatures, and therefore, these experimental studies will be used in this work for comparison purposes. This disagreement concerning the curvature in the Arrhenius plot is probably simply because the experimental measurements were performed independently over different temperature ranges. However, this reaction presents a heavy−light−heavy (HLH) mass combination, which is a good candidate to present a large tunneling effect at low temperatures and, therefore, curvature in the Arrhenius plot. Obviously, this effect will become more patent when a larger range of temperatures are simultaneously analyzed.

The extensive experimental literature on the $NH_3 + O$ reaction contrasts with the lack of theoretical studies. As far as we know, surprisingly, this reaction has not been theoretically studied, because the transition-state theory calculations of Salimian et al.[14] and Cohen[17] are really empirical approximations. The reason could be that this reaction is particularly challenging because, for the H-atom abstraction reaction, the approach of the $O(^3P)$ to ammonia with C_s symmetry proceeds over two potential energy surfaces (PESs), $^3A'$ and $^3A''$. Indeed, for C_s symmetry the irreducible representation is $^3A' + {}^3A''$ for reactants and $^3A' + {}^3A'' + {}^1A' + {}^1A''$ for products, and therefore, both asymptotes adiabatically correlate through the PESs $^3A'$ and $^3A''$ in C_s.

In this paper, we focus on the H-atom abstraction reaction. We first calculate the energy, geometry, and vibrational frequencies of the stationary points by using electronic structure calculations. In a second step, we use ab initio information in the region along the reaction-path, which is usually referred to as a "direct dynamics" method.[19] This method describes a chemical reaction by using ab initio information (energies, gradients, and Hessians) only in the region of configuration

* E-mail: joaquin@unex.es.

10.1021/jp000908b CCC: $19.00
Published on Web 07/20/2000

space along the reaction-path and has yielded satisfactory results for some hydrogen abstraction reactions.[19−28] To obtain kinetic information, we perform variational transition-state theory (VTST) calculations with the inclusion of multidimensional tunneling effects on both the $^3A'$ and $^3A''$ surfaces independently.

2. Methods and Computational Details

2.1. Electronic Calculations. Geometry, energy, and first and second energy derivatives were calculated using the GAUSSIAN 94 system of programs.[29] The stationary point geometry [reactants, saddle points ($^3A'$ and $^3A''$ symmetry), hydrogen-bonded in the product channel (HBP), and products] was optimized at three levels of calculation: (i) restricted (R) or unrestricted (U) second-order Møller−Plesset perturbation theory,[30] MP2, with full electron correlation, using the 6-31G-(d,p) basis set;[31] (ii) the coupled-cluster approach including a perturbative estimate of connected triple excitations,[32] CCSD-(T), using the correlation-consistent polarized valence double-ζ set, cc-pVDZ, developed by Dunning et al.;[33] and (iii) density functional theory (DFT), where the exchange and correlation were treated by the B3LYP method,[34] which is based on Becke's three-parameter hybrid method[35] for combining Hartree−Fock exchange with a local density approximation exchange-correlation functional,[36] using the cc-pVTZ (triple-ζ) basis set.[33]

In a second step, to improve the energy description of the stationary points (reaction energy and barrier height), we made a single-point calculation at higher levels:

Level 1. Using the MP2/6-31G(d,p) optimized geometries, we made a single-point calculation with the CCSD(T) method using the cc-pVTZ basis set of Dunning et al. We denote this energy as

CCSD(T)/cc-pVTZ//(R-U)MP2/6-31G(d,p)

where the double slash (X//Y) denotes geometry optimization at level Y and energy calculated at level X.

Level 2. Continuing with the CCSD(T) approach, we increased the basis set using the augmented-cc-pVTZ basis set of Dunning et al., AUG-cc-pVTZ. We denote this energy as

CCSD(T)/AUG-cc-pVTZ//(R-U)MP2/6-31G(d,p)

Level 3. Using the B3LYP/cc-pVTZ optimized geometries, we made a single-point calculation with the same method, but increasing the basis set. We denote this energy as

B3LYP/AUG-cc-pVTZ//B3LYP/cc-pVTZ

To examine the performance of the results obtained with these single-reference electron correlation methods, Lee and Taylor[37] proposed the T_1 diagnostic: $T_1 = ||t_1||/N^2_{\text{elec}}$, where $||t_1||$ is the Euclidian norm of the coupled-cluster with single and double excitation amplitudes and N_{elec} is the number of active electrons in the correlation procedure. It has been suggested[37,38] that a large T_1 value (i.e., $T_1 > 0.02$) is an indication that nondynamical electron correlation effects are important and, therefore, a multireference electron correlation treatment would be more suitable. In the present case, we obtained $T_1 = 0.02$ for both $^3A'$ and $^3A''$ saddle points, a value which indicates dynamical correlation behavior for this electronic system, and, thus, the use of single-reference electron correlation methods seems to be justified, although it can be considered as a limit case.

The use of a multireference electron correlation method, even only for the stationary points, is beyond the scope of this work, and the calculation of analytical gradients along the reaction-path is an enormous computational task and is not available in any computer program package of which we are aware. However, for comparison only, we would mention two recent papers[39,40] where some single reference and multireference correlation methods have been analyzed for the similar $CH_4 + O(^3P)$[39] and $CH_4 + OH$[40] reactions, respectively. These papers clearly show that the transition state has a much greater multiconfigurational character than reactants and products and that the multireference electron correlation calculation provides a balanced treatment of dynamical and nondynamical correlation for open-shell transition states, while, from the numerical point of view, for the barrier height and reaction energy, the most expensive multireference method gives results similar to those of the single-reference methods when elaborate correlated wave functions and large basis sets are used, for example, as in the scaling of all correlation (SAC) method (see Table 5 of ref 39 and Table 3 of ref 40 using the SAC values from ref 41).

At the MP2/6-31G(d,p) level, we constructed the "intrinsic reaction coordinates" (IRCs) or minimum energy paths (MEPs) for both $^3A'$ and $^3A''$ surfaces independently, starting from the respective saddle point geometries and going downhill to both the asymptotic reactant and product channels in mass-weighted Cartesian coordinates with a gradient step size of 0.1 bohr amu$^{1/2}$. Along these MEPs the reaction coordinate, s, is defined as the signed distance from the saddle point, with $s > 0$ referring to the product side. In the rest of the work the units of s are bohr, and the reduced mass to scale the coordinates[42] is set to 1 amu. This has no effect on calculated observables, but it does affect the magnitude of s in plots used for interpretative purposes. In addition, for 20 points along these MEPs we computed the gradients and Hessians at this level, avoiding all the time undesirable reorientations of molecular geometries.

2.2. Dynamics. For the $^3A'$ and $^3A''$ surfaces, independently, at the points along the MEPs, we perform a generalized normal-mode analysis, projecting out frequencies at each point along the path.[43] With this information, we calculated, first, the ground-state vibrationally adiabatic potential curve

$$V_a^G(s) = V_{\text{MEP}}(s) + \epsilon_{\text{int}}^G(s) \quad (1)$$

where $V_{\text{MEP}}(s)$ is the classical energy along the MEP with its zero energy at the reactants ($s = -\infty$) and $\epsilon_{\text{int}}^G(s)$ is the zero-point energy at s from the generalized normal-mode vibrations orthogonal to the reaction coordinate, and second, the coupling terms,[40] $B_{k,F}(s)$, measuring the coupling between the normal mode k and the motion along the reaction coordinate, mode F. These coupling terms are the components of the reaction-path curvature, $\kappa(s)$, defined as

$$\kappa(s) = \left(\sum [B_{k,F}(s)]^2\right)^{1/2} \quad (2)$$

and they control the nonadiabatic flow of energy between these modes and the reaction coordinate.[44,45] These coupling terms will allow us to calculate accurate semiclassical tunneling factors and to give a qualitative explanation of the possible vibrational excitation of reactants and/or products, that is, dynamical features.

Finally, the energies, vibrational frequencies, geometries, and gradients along the MEP were used to estimate rate constants along the $^3A'$ and $^3A''$ surfaces by using variational transition state theory (VTST). We calculated thermal rates using the canonical variational theory[46,47] (CVT) approach, which locates the dividing surface between reactants and products at a point $s^{*,\text{CVT}}(T)$ along the reaction-path that minimizes the generalized TST rate constants, $k^{\text{GT}}(T,s)$, for a given temperature T. Thermodynamically, this is equivalent to locating the transition

TABLE 1: Reactant and Product Properties

	NH_3			NH_2			OH		
	MP2[a]	CCSD(T)[b]	B3LYP[c]	MP2[a]	CCSD(T)[b]	B3LYP[c]	MP2[a]	CCSD(T)[b]	B3LYP[c]
					Geometry[d]				
R(N−H)	1.011	1.027	1.014	1.023	1.041	1.028			
∠(HNH)	106.1	103.5	106.4	102.7	100.6	102.7			
R(OH)							0.971	0.980	0.974
					Frequencies[e]				
	3724(e)	3561(e)	3573(e)	3596	3415	3433	3846	3704	3699
	3566	3434	3454	3480	3319	3344			
	1728(e)	1686(e)	1677(e)	1596	1564	1542			
	1121	1181	1067						
ZPE[f]	22.3	21.6	21.5	12.4	11.9	11.9	5.5	5.3	5.3
TC[g]	1.8	1.8	1.8	1.8	1.8	1.8	1.5	1.5	1.5

[a] MP2=FULL/6-31G(d,p) level. [b] CCSD(T)/cc-pVDZ level. [c] B3LYP/cc-pVTZ level. [d] In angstroms and degrees. Experimental values are as follows.[56] $NH_3(C_{3v})$: 1.012, 106.7. $NH_2(C_{2v})$: 1.02, 103.4. $OH(C_{\infty v})$: 0.971. [e] In inverse centimeters. Experimental values are as follows.[56] NH_3: 3577(e), 3506, 1691(e), 1022. NH_2: 3220, 3173, 1497. OH: 3735. [f] Harmonic zero-point energy, in kilocalories per mole; the harmonic ZPE is one-half the sum of the frequencies for the bound modes. [g] Thermal corrections at 298 K.

state at the maximum $\Delta G^{GT,\circ}[T,s^{*,CVT}(T)]$ of the free energy of activation profile $\Delta G(T,s)$.[46,47] Thus, the thermal rate constant will be given by

$$k^{CVT}(T) = \sigma\frac{k_B T}{h}K^\circ \exp[-\Delta G(T,s^{*,CVT})/k_B T] \qquad (3)$$

with k_B being Boltzmann's constant, h being Planck's constant, σ being the symmetry factor (the number of equivalent reaction-paths, which were assumed to be 3 and 2 for the forward and reverse reactions, respectively), and K° being the reciprocal of the standard-state concentration, taken as 1 molecule cm^{-3}.

In the present work, we used the general polyatomic rate constants code POLYRATE.[48] The rotational partition functions were calculated classically, and the vibrational modes were treated as quantum-mechanical separable harmonic oscillators, with the generalized normal modes defined in redundant curvilinear coordinates.[49,50] The chosen curvilinear coordinates were all the possible bond lengths and bond angles. The advantage of curvilinear coordinates (nonlinear functions of Cartesian coordinates) over rectilinear ones (linear functions of Cartesian coordinates) is that, in some cases, the lowest bending frequencies had unphysical imaginary values over a wide range of the reaction coordinate using rectilinear coordinates, whereas these frequencies were real over the whole of the reaction-path using curvilinear coordinates. This behavior has been verified in the title reaction and other hydrogen abstraction reactions.[51−53] In calculating electron partition functions, we included the spin−orbit splitting of $O(^3P)$, which is 158.26 and 226.98 cm^{-1} for $^3P_1$ and $^3P_0$ relative to $^3P_2$. We also included the two electronic states for the OH product in the calculation of its electronic partition function, with a 140 cm^{-1} splitting. We also consider the tunneling contribution. As we have information only on the reaction-path, centrifugal-dominant small-curvature tunneling (SCT)[51] is used. Methods for large-curvature cases have been developed,[55] but they require more information about the PES than was determined in the present study. Finally, the total rate constant is obtained from the sum of the calculated rate constants for the $^3A'$ and $^3A''$ surfaces.

3. Results and Discussion

3.1. Structures and Vibrational Frequencies. On the two PESs ($^3A'$ and $^3A''$) the reaction of the O atom with ammonia proceeds via a saddle point and a hydrogen-bonded complex (HBP) in the product channel. The optimized geometries and harmonic vibrational frequencies of reactants and products are listed in Table 1, and those of the saddle points ($^3A'$ and $^3A''$) and HBP are listed in Table 2. With respect to the experimental geometries of reactants and products, the CCSD(T) and B3LYP methods overestimate the bond lengths, while the MP2 level reproduces these geometries better. With respect to the harmonic frequencies, the behavior is the reverse. Thus, the CCSD(T) and B3LYP methods agree with the experimental values, while the MP2 level is an overestimate. However, the differences found at this level balance out between reactants and products.

Next we consider the saddle point, whose geometrical structure, NH_3O, is shown in Figure 1. When the $O(^3P)$ approaches the NH_3 with C_s symmetry, we obtain two electronic states of symmetries $^3A'$ and $^3A''$ with different energies (see below): the $^3A'$ with the half-filled p-orbital in the NH_1O plane, and the $^3A''$ with the half-filled p-orbital perpendicular to the plane. For the $^3A'$ surface, the length of the bond that is broken ($N-H_1$) increases by 19%, 21%, and 25%, at the MP2, CCSD(T), and B3LYP levels, respectively, and the length of the bond that is formed (H_1-O) increases by 21%, 20%, and 19%, respectively. In all cases, these results indicate that the barrier is almost centrally located, as expected for a weakly endothermic reaction. At the three levels, the saddle point presents a "bent" structure, that is, an $N-H_1-O$ angle different from 180°. The saddle point at each level was identified with one negative eigenvalue of the respective Hessian matrix and, therefore, one imaginary frequency. The MP2 method (1724i cm^{-1}) presents an absolute value greater than that of the B3LYP method (1456i cm^{-1}). It is noteworthy to point out that, at the CCSD(T) level, an SCF convergence in energy was not found and, hence, vibrational frequencies could not be determined either. The fact that the GAUSSIAN 94 program package computes numerical (and not analytical) second derivatives at this level might account for this divergence. Several trials with different step sizes (from 0.01 to 0.0001 Å) for the numerical second-derivative calculations did not improve this situation.

For the $^3A''$ saddle point, the length of the bond that is broken ($N-H_1$) increases by 21%, 21%, and 25% at the MP2, CCSD(T), and B3LYP levels, respectively, and the length of the bond that is formed (H_1-O) increases by 20%, 20%, and 19%, respectively, indicating in all cases that the barrier is also almost centrally located, as in the $^3A'$ saddle point. At the three levels, the saddle point also presents a "bent" structure, with angles from 144.4° to 150.5°. Therefore, the $^3A''$ saddle point is more "bent" than the $^3A'$ one. The imaginary frequency is 1304i and 1416i cm^{-1}, at the MP2 and B3LYP levels, respectively.

TABLE 2: Saddle Point and Hydrogen-Bonded Product Complex Properties[a]

	SP(^{3}A′)			SP(^{3}A″)			HBP		
	MP2	CCSD(T)	B3LYP	MP2	CCSD(T)	B3LYP	MP2	CCSD(T)	B3LYP
					Geometry				
$R(NH_1)$	1.200	1.243	1.266	1.220	1.245	1.266	2.024		1.960
$R(OH_1)$	1.175	1.173	1.155	1.166	1.181	1.163	0.978		0.985
$\angle(NH_1O)$	159.5	161.9	165.9	144.4	146.0	150.5	180.0		180.0
$R(NH)$	1.020	1.036	1.022	1.020	1.034	1.021	1.021		1.025
$\angle(H_1NH)$	103.3	100.0	104.5	106.1	102.8	107.6			
					Frequencies				
	3631		3500	3644		3511	3716		3497
	3517		3405	3535		3423	3630		3474
	1630		1796	1662		1586	3512		3380
	1600		1560	1513		1327	1595		1536
	1300		1145	1222		1069	601		609
	847		760	882		762	554		534
	586		560	528		469	211		194
	513		490	506		429	192		166
	1724i		1456i	1304i		1416i	165		157
ZPE	19.5		18.9	19.3		18.0	20.3		19.4
TC	2.1		2.1	2.1		2.2	3.1		3.1

[a] As in Table 1. H_1 is the transferred atom (see Figure 1).

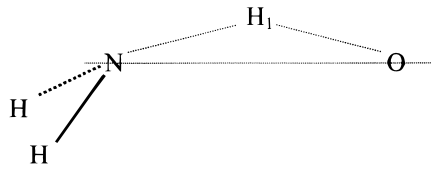

Figure 1. Definition of internal coordinates at the intermediate stationary points.

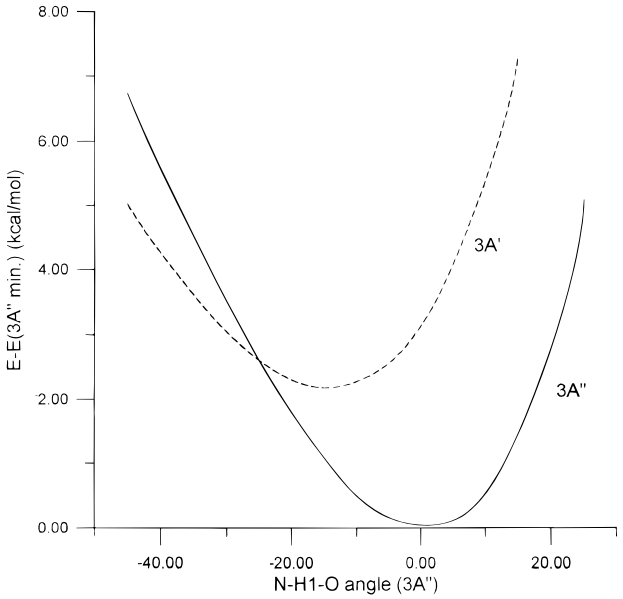

Figure 2. Energy profile for the ^{3}A′ and ^{3}A″ potential energy curves with respect to their minima at the MP2/6-31G(d,p) level. For these calculations, the other internal coordinates were fixed at their respective values in the minimum. The zero value on the *x*-axis corresponds to the N−H_1−O angle of the ^{3}A″ saddle point.

To get a clearer view of the ^{3}A′ and ^{3}A″ surfaces, we have carried out electron calculations at the MP2/6-31G(d,p) level, varying the angle N−H_1−O in relation to its respective optimized saddle point geometry. Figure 2 shows the calculations of the PESs in C_s symmetry, where all values (angles and energies) are referred to the most stable ^{3}A″ structure, and the internuclear distances, d(N−H_1) and d(H_1−O), are fixed. The two surfaces cross at a N−H_1−O angle of 169.4°, and thus, the dynamics for the ^{3}A′ and ^{3}A″ surfaces could be calculated independently.

TABLE 3. Energy and Enthalpy Changes Relative to Reactants (kcal mol^{-1}) at Various Levels

	SP(^{3}A′)	SP(^{3}A″)	HBP	P[a]
ΔE[b]	21.4	19.2	6.1	13.4
	16.1	15.0	3.5	9.9
	15.1	13.9	2.7	8.8
	5.8	4.3	-1.0	4.9
ΔH(0 K)	18.6	16.2	4.1	9.0
	13.3	12.0	1.5	5.5
	12.3	10.9	0.7	4.4
	3.0	1.3	-3.0	0.5
ΔH(298 K)	17.2	14.9	3.7	8.8
	11.9	10.7	1.1	5.3
	10.9	9.6	0.3	4.2
	1.6	0.0	-3.3	0.3

[a] Products. The experimental enthalpy of reaction value (298 K) = 4.5 kcal mol^{-1}, from the following enthalpies of formation: NH_3, −10.98 kcal mol^{-1} (ref 56); O, 59.57 kcal mol^{-1} (ref 56); OH, 9.3 kcal mol^{-1} (ref 56); NH_2, 43.8 ± 0.6 kcal mol^{-1} (ref 57). [b] For each magnitude, the first row corresponds to the MP2 level; the second to level 1, the third to level 2, and the last to level 3.

Finally, another stationary point is located in the exit channel. It is characterized as a hydrogen-bonded complex (HBP) with a bond distance (N···H_1) of 2.024 and 1.960 Å at the MP2 and B3LYP levels, respectively. The stretching frequency of HO (3846 cm^{-1} at the MP2 level) is shifted to a lower frequency by 130 cm^{-1}, and it increases in intensity from 7.32 to 266.6 km mol^{-1}. At the B3LYP level, the behavior is similar.

3.2. Energy Properties. Table 3 summarizes the energy and enthalpy changes of all the stationary points relative to the reactants at various levels.

First, we analyze the enthalpy of reaction, which can be obtained from the reactant and product enthalpies of formation at 298 K. However, the NH_2 radical presents a lack of coincidence between proposed experimental values, varying between 44.0 ± 2.3 kcal mol^{-1} (ref 58) and 48.1 ± 3.5 kcal mol^{-1} (ref 59), and the JANAF tables[56] recommend 45.5 ± 1.5 kcal mol^{-1}. Due to this lack of coincidence, we calculated this enthalpy of formation using very high ab initio levels[57] and proposed a value of 43.8 ± 0.6 kcal mol^{-1}. Using this value, the reaction enthalpy for the title reaction at 298 K is 4.5 kcal mol^{-1}. The MP2 level and level 3 (B3LYP method) yield strong

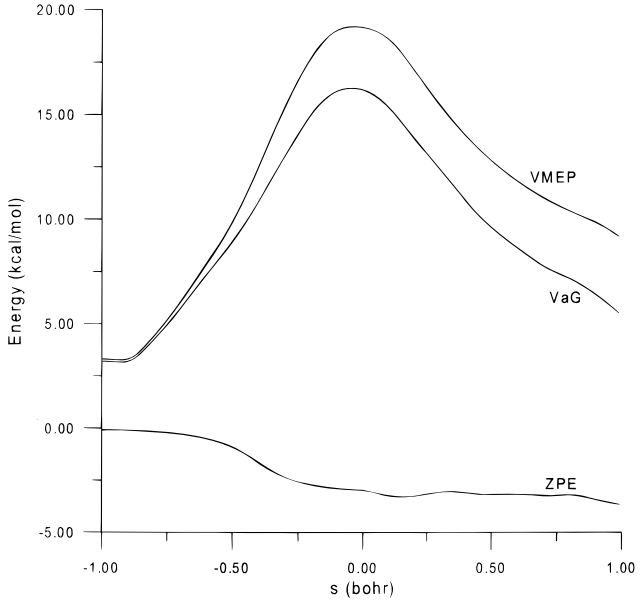

Figure 3. Classical potential energy curve (V_{MEP}), zero-point energy (ΔZPE), and vibrationally adiabatic potential energy curve (ΔV_a^G) with respect to the reactants as a function of *s*.

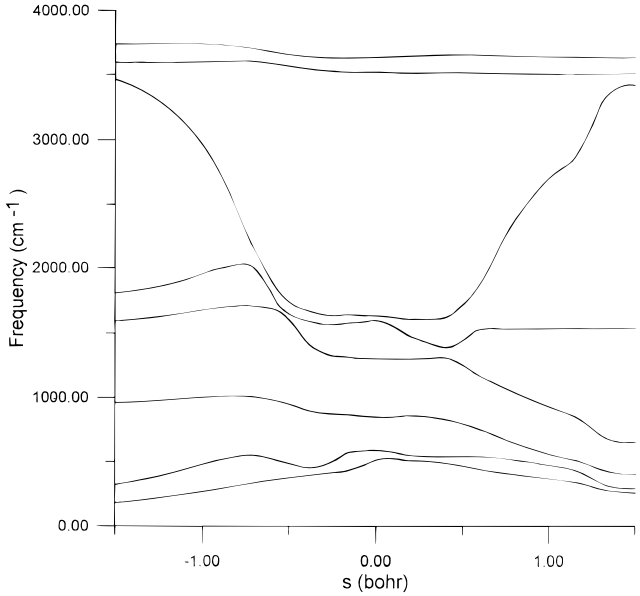

Figure 4. Generalized normal-mode vibrational frequencies plotted versus *s*.

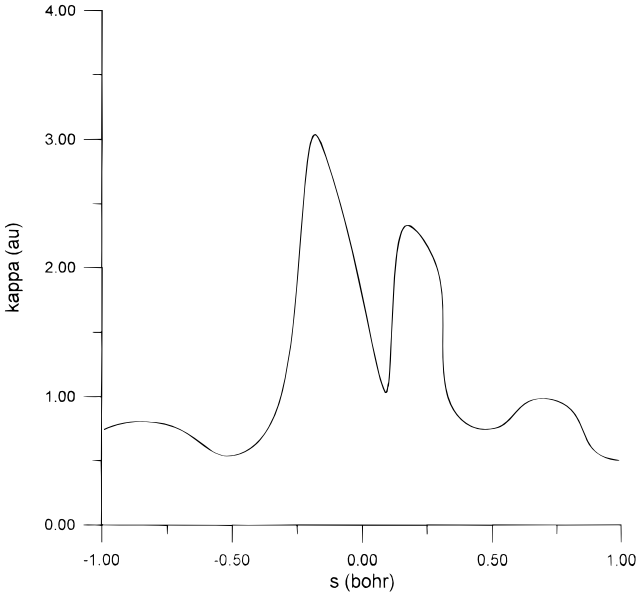

Figure 5. Curvature of the reaction-path (κ factor) as a function of *s*.

overestimates and underestimates, respectively, for this value. Thus, these levels are not adequate to represent the energetics of this reaction. Level 1 slightly overestimates the enthalpy of reaction, while level 2 yields the best agreement with the experimental data.

With respect to the barrier height, a direct comparison of theory with experiment is not possible. As we raise the calculation level (MP2 → level 2), the barrier height is lowered drastically (by 5.3 kcal mol^{-1}), and in accordance with the behavior for the enthalpy of reaction, we take level 2 as the highest level in this work. At this level 2, the $^3A''$ saddle point is 1.2 kcal mol^{-1} more stable than the $^3A'$ one, and this tendency between the $^3A'$ and $^3A''$ surfaces is reproduced at all levels. Note that level 3 (B3LYP) yields a barrierless reaction at 298 K on the $^3A''$ surface.

Finally, at level 2 the HBP is 6.1 kcal mol^{-1} (3.9 kcal mol^{-1} at 298 K) more stable than the products. In summary, there are three pieces of evidence that justify the nature of this hydrogen-bonded complex: the geometric length of $N-H_1$ (2.024 Å), the stability (3.9 kcal mol^{-1} relative to products), and, finally, the shift to lower values of the stretching frequency of the OH radical (the proton donor). These results are the typical behavior of hydrogen bond systems.

3.3. Reaction-Path Analysis. The reaction-path analysis is carried out on the information at the MP2/6-31G(d,p) level (energies, gradients, and Hessians) for the $^3A'$ and $^3A''$ surfaces. The two surfaces present similar behavior, and further discussion in this paper will refer only to the $^3A''$ surface. Figure 3 shows the classical energy along the MEP, V_{MEP}, the ground-state vibrationally adiabatic potential energy curve, ΔV_a^G, and the change in the local zero-point energy, ΔZPE, as a function of *s* over the range -1.0 to $+1.0$ bohr. Note that ΔV_a^G and ΔZPE are defined as the difference between these magnitudes at *s* and their values for the reactants.

The vibrational frequencies along the MEP are shown in Figure 4. The mode related to the breaking $(N-H_1)$/forming(H_1-O) bonds drops dramatically near the saddle point (*reactive mode*). This mode presents a widening of the vibrational well, an effect which has been found in other reactions with a small skew angle.[24,28,60] The two lowest vibrational frequencies along the reaction-path (*transitional modes*) correspond to the transformation of free rotations or free translations of the reactant limit into real vibrational motions in the global system. Their frequencies tend asymptotically to zero at the reactant and product limits and reach their maximum in the saddle point zone. Therefore, in the saddle point region, the behavior of these transitional modes only partially compensates the fall in the ZPE caused by the reactive mode, and as a result the ZPE shows noticeable changes with *s* (Figure 3).

Further analyzing the reaction valley, the curvature term (κ) of the reaction-path as a function of *s* is plotted in Figure 5, which permits us to give a qualitative analysis of the vibrational excitation of reactants and products. There are two peaks, one on the reactant side, which has a value of 3.03 au at $s = -0.18$ bohr, and one on the product side of the saddle point, which has a value of 2.32 au at $s = +0.18$ bohr. The first is due to strong coupling of the reaction-path to the NH_3 reactive stretch ($B_{k,F} = 1.50$ au) and umbrella ($B_{k,F} = 2.60$ au) modes. Excitation

of these modes might be expected to enhance the forward reaction rates. The second peak is in the exit channel and is lower than the first. It is due to the coupling of the reaction-path to the OH stretch ($B_{k,F} = 1.09$ au) and the NH_2 bend ($B_{k,F} = 2.00$ au) modes. This might be an indication that the OH stretching and the NH_2 bend modes could appear vibrationally excited. However, because of the stability of the hydrogen-bonded complex (HBP) formed, the system remains in the complex situation for a certain time before evolving to the separated products. In this short lifetime of the bonded complex, there is a transfer of energy between several modes, diminishing the OH and NH_2 excitations. When the system finally escapes from the well, this randomization of the energy will lead to OH and NH_2 excitations smaller than those in other direct reactions without the possibility of such an effective randomization. Unfortunately, a comparison with experiment is not possible.

3.4. Improved Reaction-Path. The poor agreement obtained with the MP2 level (see section 3.2 and Table 3) means that we have to optimize our ab initio reaction-path. In the following, we shall describe three methods to improve the reaction-path, which have already been used in other hydrogen abstraction reactions.[23,24,61]

Approximation 1: To lower the height of the barrier while maintaining the shape of the original MP2 curve [recall that the only reaction-path calculated had been at the MP2/6-31G-(d,p) level], we scale the MP2 curve regularly by a factor

$$F = \Delta E(\text{MP2}, s = 0)/\Delta E(\text{level 2}, s = 0) \qquad (4)$$

where ΔE is the variation of energy at each level with respect to the reactants. At the saddle point, $s = 0$, the barrier height is that of the highest level, level 2. This factor is 0.707 and 0.724 for the $^3A'$ and $^3A''$ surfaces, respectively.

Approximation 2: An alternative is to use the following scaling:

$$E_{\text{scaled},s} = \Delta E(\text{MP2}, s) + [\Delta E(\text{level 2}, s = 0) - \Delta E(\text{MP2}, s = 0)] \qquad (5)$$

However, if the difference between the highest level and the MP2 values is large, it may happen that the scaled energy at some point s close to the reactants or products is less than that of the minimum, with the appearance of fictitious minima. This is the case in this reaction at the entry channel. To avoid this problem, we take the level 2 energy close to the minima.

Approximation 3: The two previous approximations are based on the saddle point energy only, whereas in this approximation we use the VTST-ISPE (variational transition state theory with interpolated single-point energies) method,[61] in which a few extra energies calculated with a higher level theory along the lower level reaction-path are used to correct the classical energy profile of the reaction. In this case, we use the saddle point and two extra points near the saddle point using the highest level, level 2.

Figure 6 shows the classical energy along the MEP at the MP2 level, approximation 1 (MP2*F), approximation 2 (MP2-scaled), and approximation 3 (ISPE), with respect to the reactants for the $^3A''$ reaction-path. Approximation 1 lowers the barrier height while retaining the shape of the original curve, while approximation 2 also lowers the barrier height but yields a thinner barrier and, consequently, a larger tunneling effect. Approximation 3 shows an intermediate behavior.

3.5. Rate Constants. In the canonical version of VTST, CVT, the dividing surface is varied along the reaction-path to minimize the rate constants, obtaining the generalized transition state (GTS) at the value s*. Thermodynamically, the minimum rate constant criterion is equivalent to maximizing the generalized standard state free energy of activation, $\Delta G^{GT,\circ}(T,s)$, eq 3. Therefore, the effects of the potential energy, entropy, and temperature on the location of this GTS must be considered. In the present case, the bottleneck properties of the reaction, based on the CVT approach, show that the location of the GTS is very close to the saddle point: from 0.010 to 0.019 bohr for the $^3A'$ surface and from −0.060 to −0.012 bohr for the $^3A''$ surface over the temperature range 500−2000 K, respectively. Thus, the variational effects, that is, the ratio between variational CVT and conventional TST rate constants, are very small. Therefore, for this reaction the energy contribution dominates over the entropy contribution, even at high temperatures.

Figure 7 shows the total rate constants for the $NH_3 + O(^3P)$ reaction over the temperature range 500−2000 K for the three approximations used in this paper to scale the MEP, together with the experimental values from Perry[11] (at intermediate

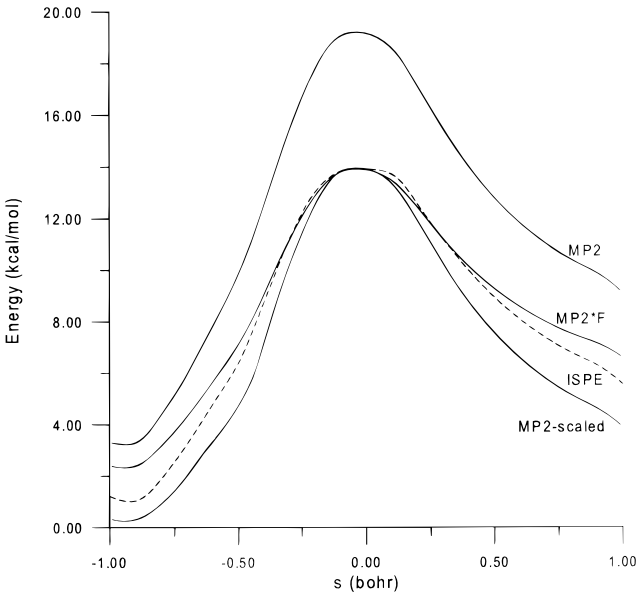

Figure 6. Potential energy curves calculated at several approximations.

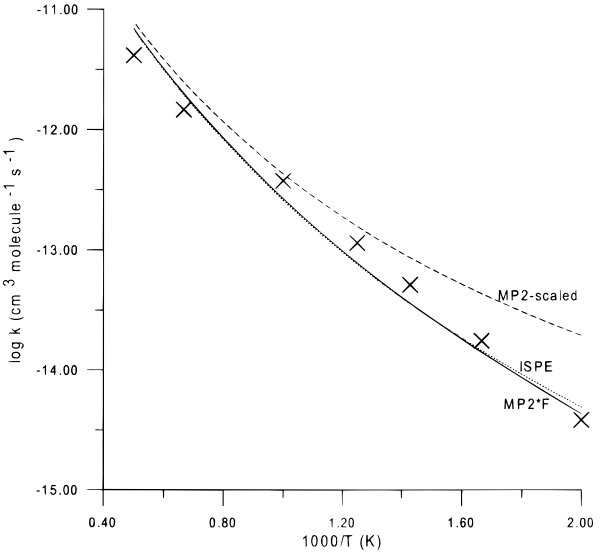

Figure 7. Arrhenius plot of log k (cm^3 molecule^{-1} s^{-1}) against the reciprocal of the temperature (K) in the range 500−2000 K. Experimental values (crosses) are from ref 11 (at intermediate temperatures, 500−1000 K) and from ref 14 (at high temperatures, 1500−2000 K).

TABLE 4: Theoretical and Experimental Activation Energies (kcal mol^{-1})

This Work[a]			
500−600 K	500−1000 K	1000−1500 K	1500−2000 K
7.00	8.16	12.01	14.74
Exp (Arrhenius Linear Behavior)			
4.90[b]	6.60[c]	9.00[d]	8.85[e]

[a] Calculated using the CVT/SCT rate constants on the two $^3A'$ and $^3A''$ surfaces. [b] Wong and Porter[6] (400−600 K). [c] Kurylo et al.[8] (361−677 K). [d] Perry[11] (448−841 K). [e] Salimian et al.[14] (1750−2060 K).

temperatures, 500−800 K) and from Salimian et al.[14,16] (at high temperatures, 1000−2000 K). Note that, taken independently, the two experimental data sets[11,14,16] show linear Arrhenius plots, but as can be seen in Figure 7, taken simultaneously these data show a small curvature. Our three approximations show curvature in the Arrhenius plot, which is the expected behavior in a reaction with a heavy−light−heavy mass combination. Approximations 1 and 3 practically coincide over the whole temperature range (with a maximum difference of 10% at 500 K) and show reasonable agreement with experiments over all the temperature ranges. Approximation 2 presents a narrower reaction-path shape, with the consequent overestimate of the tunneling effect at lower temperatures. Table 4 lists the phenomenological activation energies computed as local slopes of the Arrhenius plot for the forward reaction using approximation 1. The activation energy can be obtained from total rate constants through the usual definition

$$E_a = -R\, \mathrm{d}(\ln k)/\mathrm{d}(1/T) \qquad (6)$$

which is equivalent to determining the slope of the plot in Figure 7. As the temperature increases, the activation energy also increases, which is the typical behavior for a reaction with curvature in the Arrhenius plot. At intermediate temperatures (500−1000 K), the theoretical result is close to the more recent experimental value of Perry.[11] At high temperatures (1500−2000 K), the theoretical result strongly disagrees with the experimental result of Salimian et al.[14]

Finally, to make a quantitative estimate of the role of the tunneling in the curvature of the Arrhenius plot, we fitted the results to a three-term expression of the type $AT^m \exp(-B/T)$. The resulting equation is

$$K(T) = (4.85 \times 10^{-21})T^{2.93} \exp(-2435/T)\ \mathrm{cm^3\,molecule^{-1}\,s^{-1}} \qquad (7)$$

4. Conclusions

The present work has attempted to shed some light on the hydrogen abstraction $NH_3 + O(^3P)$ reaction, which is important in combustion and atmospheric chemistry. Experimentally, the curvature in the Arrhenius plot is still an open question. The present calculations show that tunneling plays an important role in this reaction and, therefore, a noticeable curvature can be expected in the Arrhenius plot. These theoretical results suggest that further experimental research over a wide temperature range is necessary to validate the hydrogen abstraction mechanism in the 500−2000 K range.

With respect to the stationary points, the $^3A'$ and $^3A''$ saddle points with C_s symmetry are "bent", with N−H_1−O angles of 159.5° and 144.4°, respectively. The enthalpy of reaction and the barrier height strongly depend on the level of calculation and basis set, and to reproduce the experimental data (enthalpy of reaction), highly correlated wave functions and very large basis sets are necessary, with the consequent high computational costs. At the highest level used in this work, the $^3A''$ saddle point is 1.2 kcal mol^{-1} more stable than the $^3A'$ saddle point.

We qualitatively showed that vibrational excitation of the NH_3 stretch and bend modes might be expected to enhance the forward rates and that the OH stretch and NH_2 bend modes could appear vibrationally excited. However, this excitation energy is randomized because of the time that the system exists as a hydrogen-bonded complex before evolving to separated OH and NH_2 products. As a consequence, the OH stretch and NH_2 bend modes will be less excited than those in other direct reactions.

Acknowledgment. I am grateful to Dr. D. G. Truhlar, Dr. F. Higes, and Dr. J. C. Corchado for their helpful discussions. This work was partially supported by Junta de Extremadura (Project IPR99-A009), and Ministerio de Educación y Cultura (Spain) (Project PB98-0998).

References and Notes

(1) Song, Y. H.; Blair, D. W.; Simiuski, V. J.; Bartok, W. *Eighteenth Symposium (International) on Combustion*; The Combustion Institute: Pittsburgh, PA, 1981; p 53.
(2) Fenimore, C. P.; Jones, G. W. *J. Phys. Chem.* **1961**, *65*, 298.
(3) Avramenko, L. I.; Kolesnikova, R. V.; Kuzntsova, N. L. *Izv. Akad. Nauk. SSSR, Ser. Khim.* **1962**, 983.
(4) Wong, E. L.; Potter, A. E. *J. Chem. Phys.* **1963**, *39*, 2211.
(5) Aganesyan, K. T.; Nalbandyan, A. B. *Dokl. Akad. Nauk. SSSR* **1965**, *160*, 62.
(6) Wong, E. L.; Potter, A. E. *J. Chem. Phys.* **1965**, *43*, 3371.
(7) Albers, E. A.; Hoyermann, K.; Wagner, H. G.; Wolfrum, J. *12th Symp. (Int.) Combust.* **1969**, 313.
(8) Kurylo, M. J.; Hollinden, G. A.; LeFevre, H. F.; Timmons, R. B. *J. Chem. Phys.* **1969**, *51*, 4497.
(9) Kirschner, K.; Mergete, N.; Schmidt, C. *Chem.-Ing.-Tech.* **1974**, *46*, 661.
(10) Lalo, C.; Vermiel, C. *J. Chim. Phys. Phys. Chim. Biol.* **1980**, *77*, 131.
(11) Perry, R. A. *Chem. Phys. Lett.* **1984**, *106*, 223.
(12) Baulch, D. L.; Campbell, I. M.; Hainsworth, R. *J. Chem. Soc., Faraday Trans.* **1984**, *80*, 2525.
(13) Fujii, N.; Sato, H.; Fujimoto, S.; Hiyama, H. *Bull. Chem. Soc. Jpn.* **1984**, *57*, 277.
(14) Salimian, S.; Hanson, R. K.; Kruger, C. H. *Int. J. Chem. Kinet.* **1984**, *16*, 725.
(15) Fujii, N.; Chita, K.; Uchida, S.; Hiyama, H. *Chem. Phys. Lett.* **1986**, *127*, 141.
(16) Hanson, R. K.; Salimian, S. In *Combustion Chemistry*; Gardiner, W. C., Ed.; Springer-Verlag: New York, 1985; Chapter 6, p 361.
(17) Cohen, N. *Int. J. Chem. Kinet.* **1987**, *19*, 319.
(18) Baulch, D. L.; Cobos, C. J.; Cox, R. A.; Esser, C.; Frank, P.; Just, T.; Kerr, J. A.; Pilling, M. J.; Troe, J.; Walker, R. W.; Warnatz, J. *J. Phys. Chem. Ref. Data* **1992**, *21*, 439.
(19) Baldridge, K. M.; Gordon, M. S.; Steckler, R.; Truhlar, D. G. *J. Phys. Chem.* **1989**, *93*, 5107.
(20) Doubleday, C.; McIver, J. W.; Page, M. *J. Phys. Chem.* **1988**, *92*, 4367.
(21) Garret, B. C.; Koszykowski, M. L.; Melius, C. F.; Page, M. *J. Phys. Chem.* **1990**, *94*, 7095.
(22) Isaacson, A. D.; Wang, L.; Scheiner, S. *J. Phys. Chem.* **1993**, *97*, 1765.
(23) Espinosa-García, J.; Corchado, J. C. *J. Chem. Phys.* **1994**, *101*, 1333.
(24) Espinosa-García, J.; Corchado, J. C. *J. Chem. Phys.* **1994**, *101*, 8700.
(25) Corchado, J. C.; Espinosa-García, J. *J. Chem. Phys.* **1996**, *105*, 3152.
(26) Espinosa-García, J.; Corchado, J. C.; Truhlar, D. G. *J. Am. Chem. Soc.* **1997**, *119*, 9891.
(27) Villá, J.; González-Lafont, A.; Lluch, J. M.; Corchado, J. C.; Espinosa-García, J. *J. Chem. Phys.* **1997**, *107*, 7266.
(28) Espinosa-García, J.; Coitiño, E. L.; González-Lafont, A.; Lluch, J. M. *J. Phys. Chem.* **1998**, *102*, 10715.
(29) Frisch, M. J.; Trucks, G. W.; Schlegel, H. B.; Gill, P. M. W.; Johnson, N. G.; Robb, M. A.; Cheeseman, J. R.; Keith, T.; Petersson, G. A.; Montgomery, J. A.; Raghavachari, K.; Al-Laham, M. A.; Zakrewski,

V. G.; Ortiz, J. V.; Foresman, J. B.; Ciolowski, J.; Stefanov, B. B.; Nanayakkara, A.; Challacombe, M.; Pemg, C. Y.; Ayala, P. Y.; Chen, W.; Wong, M. W.; Andres, V.; Replogle, E. S.; Gompers, R.; Martin, R. L.; Fox, D. J.; Binkley, J. S.; Defrees, D. J.; Baker, J.; Stewart, J. J. P.; Head-Gordon, M.; González, C.; Pople, J. A. *GAUSSIAN 94*; Gaussian, Inc.: Pittsburgh, PA, 1995.

(30) Møller, C.; Plesset, M. S. *Phys. Rev.* **1934**, *46*, 618.

(31) Hariharan, P. C.; Pople, J. A. *Theor. Chim. Acta* **1973**, *28*, 213.

(32) Bartlett, R. J. *J. Phys. Chem.* **1989**, *93*, 1697.

(33) Kendall, R. A.; Dunning, T. H.; Harrison, R. J. *J. Chem. Phys.* **1992**, *96*, 6796.

(34) Stephens, P. J.; Devlin, F. J.; Chabalowski, C. F.; Frisch, M. J. *J. Phys. Chem.* **1994**, *98*, 11623.

(35) Becke, A. D. *J. Chem. Phys.* **1993**, *98*, 5648.

(36) Lee, C.; Yang, W.; Parr, R. G. *Phys. Rev. B* **1988**, *37*, 785.

(37) Lee, T. J.; Taylor, P. R. *Int. J. Quantum Chem., Quantum Chem. Symp.* **1989**, *23*, 199.

(38) Lee, T. J.; Rice, J. E.; Scuseria, G. E.; Schaefer, H. F. *Theor. Chim. Acta* **1989**, *75*, 81.

(39) Roberto-Neto, O.; Machado, F. B. C.; Truhlar, D. G. *J. Chem. Phys.* **1999**, *111*, 10046.

(40) Kobayashi, Y.; Kamiya, M.; Hirao, K. *Chem. Phys. Lett.* **2000**, *319*, 695.

(41) Truong, T. N.; Truhlar, D. G. *J. Chem. Phys.* **1990**, *93*, 1761.

(42) Isaacson, A. D.; Truhlar, D. G. *J. Chem. Phys.* **1982**, *76*, 1380.

(43) Miller, W. H.; Handy, N. C.; Adams, J. E. *J. Chem. Phys.* **1980**, *72*, 99.

(44) Morokuma, K.; Kato, S. In *Potential Energy Surfaces and Dynamics Calculations*; Truhlar, D. G., Ed.; Plenum Publishing: New York, 1981; p 243.

(45) Kraka, E.; Dunning, T. H. In *Advances in Molecular Electronic Structure Theory*; JAI: New York, 1990; Vol. 1, p 129.

(46) Garrett, B. C.; Truhlar, D. G. *J. Am. Chem. Soc.* **1979**, *101*, 4534.

(47) Truhlar, D. G.; Isaacson, A. D.; Garrett, B. C. In *The Theory of Chemical Reactions*; Baer, M., Ed.; Chemical Rubber: Boca Raton, FL, 1985; Vol. 4.

(48) Chuang, Y. Y.; Corchado, J. C.; Fast, P. L.; Villá, J.; Coitiño, E. L.; Hu, W. P.; Liu, Y. P.; Lynch, G. C.; Nguyen, K.; Jackells, C. F.; Gu, M. Z.; Rossi, I.; Clayton, S.; Melissas, V.; Steckler, R.; Garrett, B. C.; Isaacson, A. D.; Truhlar, D. G. *POLYRATE*, Version 8.4; University of Minnesota, Minneapolis, MN, 1999.

(49) Jackels, C. F.; Gu, Z.; Truhlar, D. G. *J. Chem. Phys.* **1995**, *102*, 3188.

(50) Chuang, Y. Y.; Truhlar, D. G. *J. Phys. Chem.* **1997**, *101*, 3808.

(51) Natanson, G. A.; Garrett, B. C.; Truong, T. N.; Joseph, T.; Truhlar, D. G. *J. Chem. Phys.* **1991**, *94*, 7875.

(52) Espinosa-García, J.; Corchado, J. C. *J. Phys. Chem.* **1996**, *100*, 16561.

(53) Corchado, J. C.; Espinosa-García, J. *J. Chem. Phys.* **1997**, *106*, 4013.

(54) Lu, D. H.; Truong, T. N.; Melissas, V. S.; Lynch, G. C.; Liu, Y. P.; Garrett, B. C.; Steckler, R.; Isaacson, A. D.; Rai, S. N.; Hancock, G. C.; Lauderdale, G. C.; Joseph, T.; Truhlar, D. G. *Comput. Phys. Commun.* **1992**, *71*, 235.

(55) Truong, T. N.; Lu, D.-h.; Lynch, G. C.; Liu, Y. P.; Melissas, V. S.; Stewart, J. J.; Steckler, R.; Garrett, B. C.; Isaacson, A. D.; González-Lafont, A.; Rai, S. N.; Hancock, G. C.; Joseph, T.; Truhlar, D. G. *Comput. Phys. Commun.* **1993**, *75*, 43.

(56) *JANAF Thermochemical Tables*, 3rd ed.; Chase, M. W., Davies, C. A., Downey, J. R., Frurip, D. J., McDonald, R. A., Syverud, A. N., Eds.; National Standard Reference Data Series 14; National Bureau of Standards: Washington, DC, 1985.

(57) Espinosa-García, J.; Corchado, J. C.; Fernández, J.; Márquez, A. *Chem. Phys. Lett.* **1995**, *233*, 220.

(58) DeFrees, D. J.; Hehre, W. J.; McIver, R. T.; McDaniel, D. H. *J. Phys. Chem.* **1979**, *83*, 232.

(59) Carson, A. S.; Laye, P. G.; Yurekli, M. *J. Chem. Thermodyn.* **1977**, *9*, 827.

(60) Bondi, D. K.; Connor, J. N. L.; Garrett, B. C.; Truhlar, D. G. *J. Chem. Phys.* **1983**, *78*, 5981.

(61) Chuang, Y. Y.; Corchado, J. C.; Truhlar, D. G. *J. Phys. Chem.* **1999**, *103*, 1140.